Engineering Geology 334 (2024) 107497

Contents lists available at ScienceDirect

Engineering Geology

journal homepage: www.elsevier.com/locate/enggeo

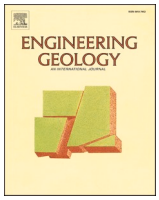

A novel framework for landslide displacement prediction using MT-InSAR and machine learning techniques

Chao Zhou [a,b], Ying Cao [c,*], Lulu Gan [a], Yue Wang [c], Mahdi Motagh [b,d], Sigrid Roessner [b], Xie Hu [e], Kunlong Yin [c]

[a] School of Geography and Information Engineering, China University of Geosciences, 430078 Wuhan, China
[b] Department of Geodesy, Section of Remote Sensing and Geoinformatics, Helmholtz Centre Potsdam, GFZ German Research Centre for Geosciences, 14473 Potsdam, Germany
[c] Faculty of Engineering, China University of Geosciences, 430074 Wuhan, China
[d] Institute for Photogrammetry and GeoInformation, Leibniz University Hannover, 30167 Hannover, Germany
[e] College of Urban and Environmental Sciences, Peking University, 100871 Beijing, China

ARTICLE INFO

Keywords:
MT-InSAR
Machine learning
Landslide displacement prediction
Deformation characteristics

ABSTRACT

The prediction of landslide deformation is an important part of landslide early warning systems. Displacement prediction based on geotechnical in-situ monitoring performs well, but its high costs and spatial limitations hinder frequent use within large areas. Here, we propose a novel physically-based and cost-effective landslide displacement prediction framework using the combination of Multi-Temporal Interferometric Synthetic Aperture Radar (MT-InSAR) and machine learning techniques. We first extract displacement time series for the landslide from spaceborne Copernicus Sentinel-1A SAR imagery by MT-InSAR. Using wavelet transform, we then decompose the nonlinear displacement time series into trend terms, periodic terms, and noises. The advanced machine learning method of Gated Recurrent Units (GRU) is utilized to predict the trend and periodic displacements, respectively. The modeling inputs for trend and periodic displacement predictions are determined by analyzing their corresponding influencing factors. The total displacements are finally predicted by summing the predicted displacements of trend and periodic items. The Shuping and Muyubao landslides, identified as seepage-driven and buoyancy-driven, respectively, in the Three Gorges Reservoir area in China are selected as case studies to evaluate the performance of our methodology. The prediction results demonstrate that machine learning algorithms can accurately establish the nonlinear relationship between the landslide deformation and its triggers. GRU outperforms the algorithms of Long Short-Term Memory networks and Kernel-based Extreme Learning Machine, and the Adam algorithm can effectively optimize the model hyperparameters. The root mean square error and mean absolute percentage error are 3.817 and 0.022 in Shuping landslide, and 5.145 and 0.020 in Muyubao landslide, respectively. By integrating the advantages of MT-InSAR and machine learning techniques, our proposed prediction framework, considering the physics principles behind landslide deformation, can predict landslide displacement cost-effectively within large areas.

1. Introduction

Landslides are among the most destructive natural hazards. They cause numerous casualties and huge property loss. The average number of annual fatalities is >4, 300 worldwide (Froude and Petley, 2018). Nearly $19.8 billion is invested to deal with the damage caused by landslide disasters each year, which accounts for 17% of the annual loss caused by the global natural disasters (Haque et al., 2016). As reported by the Ministry of Natural Resources of the People's Republic of China, 3, 919 landslides were among the 5, 659 geological disasters observed in 2022 in China (https://m.mnr.gov.cn/sj/zrzyzygb/index.html, accessed on Jan. 11, 2024). On July 23, 2019, 43 deaths, 9 missing people and an economic loss of $29 million were caused by a catastrophic landslide in Shuicheng, Guizhou province of China.

The United Nations International Strategy for Disaster Reduction addresses early warning systems as powerful tools to reduce risks in a wide range of fields including landslides (Intrieri et al., 2019). Implementing Landslide Early Warning Systems (LEWS) is a challenging task

* Corresponding author.
E-mail address: caoying@cug.edu.cn (Y. Cao).

https://doi.org/10.1016/j.enggeo.2024.107497
Received 20 April 2023; Received in revised form 30 January 2024; Accepted 7 April 2024
Available online 8 April 2024
0013-7952/© 2024 Elsevier B.V. All rights reserved.

that has attracted numerous efforts worldwide (Chae et al., 2017; Xu et al., 2020). Monitoring movements, environmental factors and geotechnical parameters play significant roles in supporting the development of LEWS. The conventional in-situ ground-based monitoring methods, such as fiber optic, piezometers, extensometers, and inclinometers, provide information for the development and implementation of LEWS (Ju et al., 2020; Fan et al., 2020).

Displacement is direct evidence of the state of landslide activity, and it is also the most primary alert used in LEWS (Pecoraro et al., 2019). Global Navigation Satellite System (GNSS) can measure landslide movement at high accuracy, while its application is limited by high cost and its point based spatial extent. For example, in the Three Gorges Reservoir Area (TGRA) in China, the frequent occurrence of new landslides and reactivation of already existing landslides are mainly caused by reservoir impoundment. There are currently 5386 known landslides in this region and only <300 of them being monitored by specialized equipment (Cheng, 2014). Statistics of worldwide fatal landslides show that the landslide-induced casualties mainly occur in less developed regions (Froude and Petley, 2018), where chances are high that local governments cannot afford the high cost of landslide monitoring and early warning. Thus, there is an urgent demand for developing methodologies and techniques contributing to cost-effective LEWS.

With the rapid development of earth observation techniques, LEWS are entering a new era (Intrieri et al., 2018; Casagli et al., 2023). Spaceborne Interferometric Synthetic Aperture Radar (InSAR) has the capability of measuring ground surface deformation over wide areas with centimeter accuracy (Zebker et al., 2010). Due to the spatio-temporal decorrelation problem of InSAR, the Multi-Temporal (MT)-InSAR method has been proposed and developed, which helps provide reliable time series of displacements for a wide range of settings (Ferretti et al., 2001; Berardino et al., 2002; Ferretti et al., 2011). In addition, due to the global coverage and open source of Sentinel-1 A imagery, MT-InSAR has become a geodetic method of choice for monitoring purposes in reducing landslide risk (Casagli et al., 2023). At present, MT-InSAR is popular in landslide detection (Rosi et al., 2018; Zhao et al., 2018; Zhang et al., 2020), landslide susceptibility mapping (Carla et al., 2016; Ciampalini et al., 2016; Devara et al., 2021), and landslide monitoring (Hu et al., 2020; Wasowski and Pisano, 2020; Xia et al., 2022). However, there are still only a few studies on the application of MT-InSAR in the context of landslide early warning.

Landslide deformation prediction is an important part of LEWS (Sassa et al., 2009; Intrieri et al., 2019). The proposed prediction models can be divided into two categories: data-driven and physically-driven. Physically-driven models forecast landslide events through mechanics principles and geotechnical parameters (Helmstetter et al., 2004). These models perform accurately, but their implementation is complex and difficult (Thiebes et al., 2014; Yang et al., 2019). The data-driven models are more attractive due to their accurate prediction and simple implementation (Zhou et al., 2018a). Machine learning (ML) have strong nonlinear fitting capabilities. Previous literature has demonstrated that ML methods can achieve excellent performance in data-driven modeling (Cao et al., 2016; Hu et al., 2021; Peng et al., 2024). The common methods utilized in landslide displacement prediction mainly include artificial neural network (Xu and Niu, 2018; Yang et al., 2019), Support Vector Machine (Cao et al., 2020; Han et al., 2021), Extreme Learning Machine (Deng et al., 2021), and Long Short-Term Memory (LSTM) networks (Yang et al., 2019).

Due to the dynamic and nonlinear characteristics of landslide deformation, accurate prediction of abrupt deformation, though challenging, is extremely important. It is required to establish the dynamic relationship between landslide displacement and its triggers (Mohanty et al., 2021). Gated Recurrent Units (GRU) algorithm is an advanced algorithm, which has been successfully applied in various fields (Zhang, 2021; Jiang et al., 2022; Zheng et al., 2022). The prediction accuracy of GRU is sensitive to its hyperparameters. Adaptive Moment Estimation (Adam) is a novel stochastic optimizer that can effectively solve the global optimization problem with large-scale hyperparameters, strong noise, and sparse gradient (Yin et al., 2021). It can be utilized to optimize the hyperparameters of the GRU model to accelerate the convergence speed and improve the training effect.

In this study, two reservoir landslides named Shuping landslide and Muyubao landslide in TGRA are selected as case studies. Based on 37 Sentinel-1A images from 10/03/2016 to 09/13/2017, the temporal and spatial pattern of displacement fields in both landslides are retrieved using MT-InSAR technique. Both landslides are characterized in temporal and spatial deformation. Based on the relationship analysis between landslide ground movement and the influencing factors, dominating factors are selected as inputs to construct the GRU displacement prediction model. We attempt to achieve cost-effective landslide monitoring and displacement prediction framework for LEWS by combining MT-InSAR and ML techniques.

2. Study areas

The Three Gorges Reservoir Area (TGRA) in China is located between Chongqing municipality and Yichang City in Hubei Province. The total bank length of the Yangtze River is about 660 km. The TGRA has a wet subtropical climate, while Summer is the season of concentrated rainfall. The TGRA began to impound water in 2003, which reached a water level of 175 m in 2008. Since then, the reservoir level fluctuation has been periodically regulated between 145 m–175 m with a sequence of stages (Fig. 1), including rising, high reservoir water level (RWL), slow drawdown, rapid drawdown, and low RWL. Landslide acceleration or failure can be easily triggered in the bank slope whose hydrogeological conditions was changed. For example, the first impoundment to 135 m and 172 m induced the failure of Qianjiangping landslide and Gongjiafang landslide, respectively. The Shuping landslide and Muyubao landslide has accelerated deformations since the first impoundment in 2003.

2.1. Shuping landslide

The Shuping landslide is located 47 km away from the Three Gorges Dam, in the Zigui County, Hubei Province in TGRA (30°59′37″N, 110°37′00″E) (Fig. 2). The Mudstone and siltstone with marl compose the main sliding mass material (Fig. 2e). The plane is fan-shaped with two gullies as the side boundaries. The altitude of the boundaries is between 60 m and 400 m above sea level (a.s.l.). The area of the Shuping landslide is about 5.5×10^5 m^2, while the volume is 2750×10^4 m^3 (Fig. 2c). Shuping landslide is currently active, and the deformation mainly occurs in the eastern and middle parts (Song et al., 2018). Upon the potential failure, it could break the 620 acres of orange forest and 800 m of roads on the landslide. The Yangtze River shipping and the residents near the bank would also be endangered by the waves generated by a potential landslide failure.

2.2. Muyubao landslide

The Muyubao landslide is also located in the Zigui County (31°01′59”N, 110°29′57″E) (Fig. 2). It has developed in a dip slope with a chair-like shape in the plane. The average slope of the landslide is 20°, while the attitude of which varies between 120 m to 425 m a.s.l.. The total volume of the Muyubao landslide is 9.0 million m^3. The detailed characteristic description of Muyubao landslide can be found in Zhou et al. (2020). Once the current movement develops into a rapid failure, the sliding mass would threaten about 140 households and 500 people lived on the landslide, as well as the ships in the Yangtze River (Huang et al., 2020).

2.3. SAR Data

Sentinel-1 is a dual-satellite constellation imaging global land and ocean. This mission provides C-band SAR data which is freely available

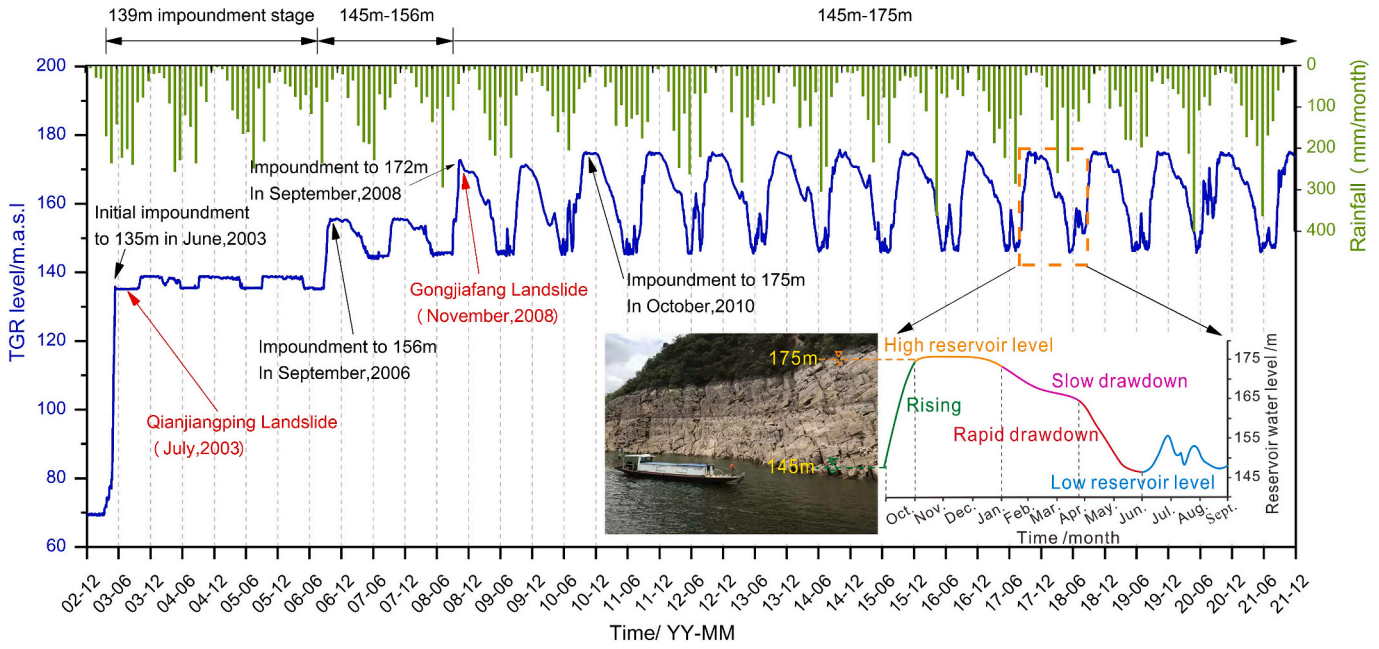

Fig. 1. Water level and precipitation in the Three Gorges Reservoir area, China.

and suitable for geohazard deformation monitoring. In this study, 37 ascending images from March 10th, 2016 to September 13th, 2017 are acquired from ESA (Fig. 3). The Precise Orbit Ephemerides and digital elevation model obtained by Shuttle Radar Topography Mission are applied to eliminate the noise and error to improve monitoring accuracy of MT-InSAR. The reservoir water level is collected by Yangtze River Water Conservancy Commission and the precipitation of Zigui County is collected from China Meteorological Administration.

3. Methodology

3.1. Overall approach of MT-InSAR-driven displacement prediction framework

Our proposed MT-InSAR-driven displacement prediction approach consists of five steps (Fig. 4): a) Extract the landslide displacement using MT-InSAR method from Sentinel-1A images (Details in Section 3.2); b) Interpolate the extracted displacement data to a same time interval, and decompose them into trend term, periodic term, and noise using wavelet transform (Details in Section 3.3); c) Train the machine learning prediction models for periodic and trend term seperately (Details in Section 3.4); d) Predict the total displacement and verify the model performance (Details in Section 3.5).

3.2. Displacement extraction using MT-InSAR

The Multi-temporal InSAR (MT-InSAR) techniques provide an effective solution for monitoring slow movements of the Earth's surface through processing multiple collections taken over time (Motagh et al., 2013; Shi et al., 2018; Bekaert et al., 2020; Zhou et al., 2022a). But its monitoring effectiveness varies with radar wavelength, satellite revisit time, and radar scattering characteristics. The Small Baseline Subset (SBAS) method is a popular method with excellent monitoring accuracy and spatial coverage density (Berardino et al., 2002; Li et al., 2022; Wang et al., 2023). In this study, interferometric processing is conducted by LiCSAR (Morishita et al., 2020). Subsequently, the landslide displacement is obtained using Stanford Method for Persistent Scatterers Multi-Temporal InSAR (StaMPS-MTI). In the SBAS implementation of StaMPS-MTI (Hooper, 2008), the targets whose filtered phase shows slow decorrelation over short time intervals are selected for time-series analysis. The candidate targets are selected based on a threshold (0.6) for the amplitude difference dispersion, which is the standard deviation of the amplitude difference between master and slave over the mean amplitude (Lubitz et al., 2012). Moreover, a three-dimensional phase unwrapping method is utilized to achieve more robust phase unwrapping. Detailed information about StaMPS-MTI method can be found in Hooper et al. (2004, 2007) and Hooper and Zebker (2007).

The original ground displacement obtained by MT-InSAR approach is along the direction of Line-of-sight (LOS) of radar satellite. To compare the monitoring results with GNSS method for validation analysis, the LOS displacement needs to be projected into the landslide movement direction. The movement directions of Shuping and Muyubao landslides are obtained through field investigation, and are N11°E and N16°E, respectively. Combining SAR image and slope geometry parameters, a popular method for projecting LOS displacement into the steepest slope direction has been proposed by Hilley et al. (2004). Here, based on this method and the obtained parameters of landslide movement direction, we project the LOS displacement into the main sliding direction.

3.3. Displacement decomposition

Landslide deformation is affected by a combination of internal geological conditions and external triggers. The internal geological conditions of a landslide encompass the geological elements which impact the initiation, evolution, and stability of a landslide. These elements mainly include the topography, the material of the sliding mass, the stratigraphy, and the hydrological conditions, etc.. The displacement primarily controlled by internal geological conditions shows a monotonic increase over time at low frequencies, defined as trend displacement. Conversely, the displacement induced by triggering factors, such as rainfall and reservoir level fluctuations, exhibits fluctuations at high frequencies, which is defined as periodic displacements. The time series of landslide displacement can be decomposed as trend displacement, periodic displacement and noise based on the principle of time series. The formula can be represented as follows:

$$D_t = T_t + P_t + N_t \quad (1)$$

where D_t is the total displacement obtained by monitoring, T_t is the

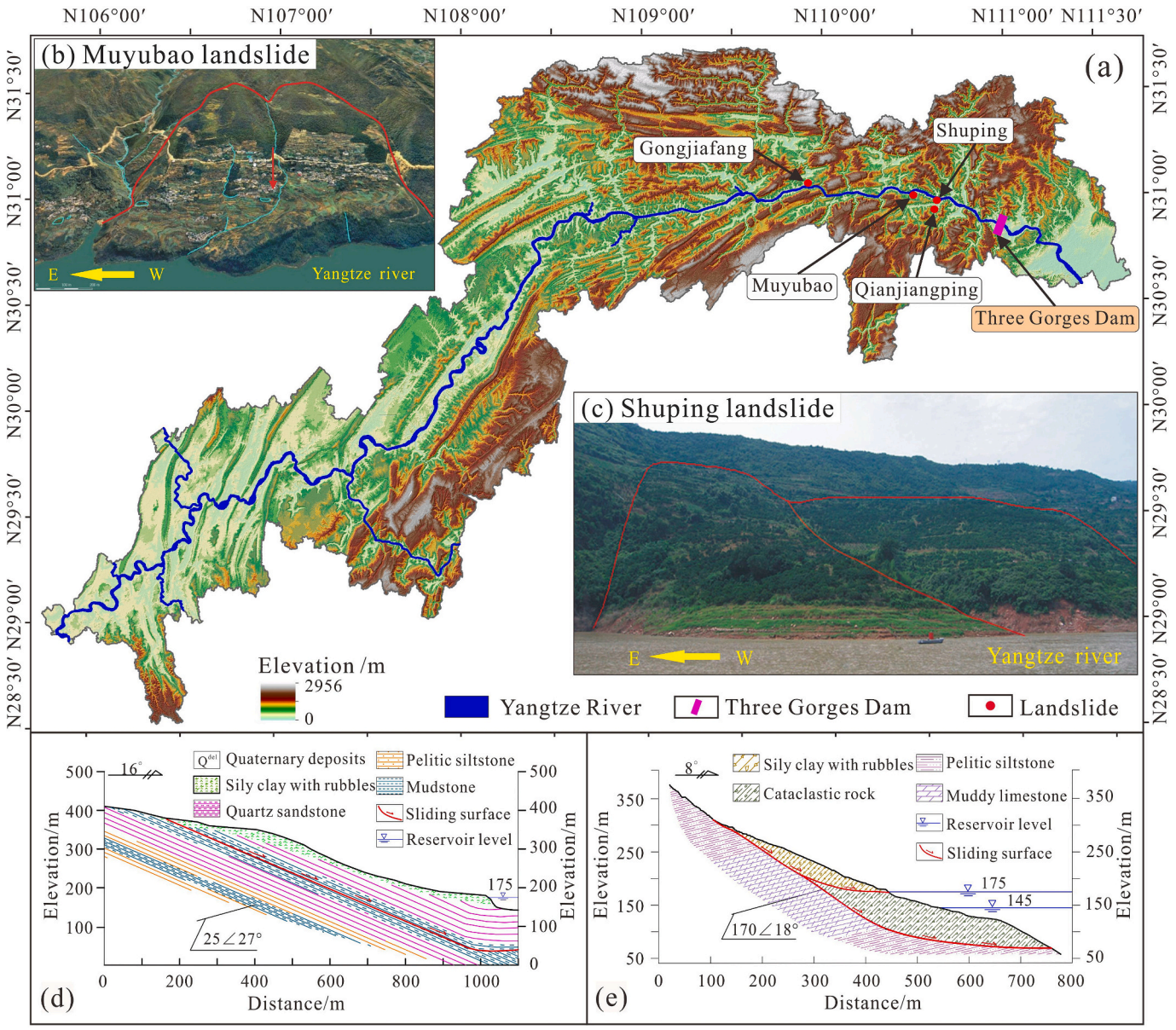

Fig. 2. (a) Location map of TGRA, with mentioned landslides' locations, (b) Landform of Muyubao landslide, (c) Landform of Shuping landslide, (d) One profile of Muyubao landslide, and (e) One profile of Shuping landslide.

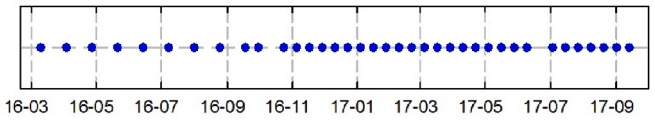

Fig. 3. Time span of sentinel-1A imagery.

trend displacement, P_t is the periodic displacement, and N_t is the noise. Sentinel-1 satellite covers the study area with a revisit time of 12 days with the exception in the beginning of 2016, when the temporal baseline of images was 24 days. This makes the time intervals of the extracted displacements irregular. We assume that the deformation velocity is constant between two adjacent monitoring. The linear interpolation is performed for the 24-day monitoring intervals to make the whole displacement sequence with the same interval of 12 days.

Wavelet decomposition algorithm (WD) can provide better localized features in both time and space domains. The discrete wavelet decomposition algorithm proposed by Mallat (1999) is an effective algorithm and popular in landslide displacement decomposition (Haghshenas Haghighi and Motagh, 2016; Guo et al., 2020; Li et al., 2020). Here, we use the one-dimensional denoising method of WD to remove the noise. Fourth-order Daubechies function (DB 4) is selected as the basis function of the discrete WD algorithm.

3.4. *Prediction modeling using GRU*

The deformation evolution of landslides is a nonlinear process controlled by various internal and external factors. In our proposed displacement prediction method, we use historical displacements for training machine learning algorithms to establish the nonlinear relationship between the landslide deformation and its triggers. The trained models are applied to predict future displacements. GRU is an advanced machine learning algorithm with strong nonlinear predictive ability. The factors affecting the displacement of the period item and the trend item are different. We determine the inputs for both models with consideration of the physics principles behind landslide deformation.

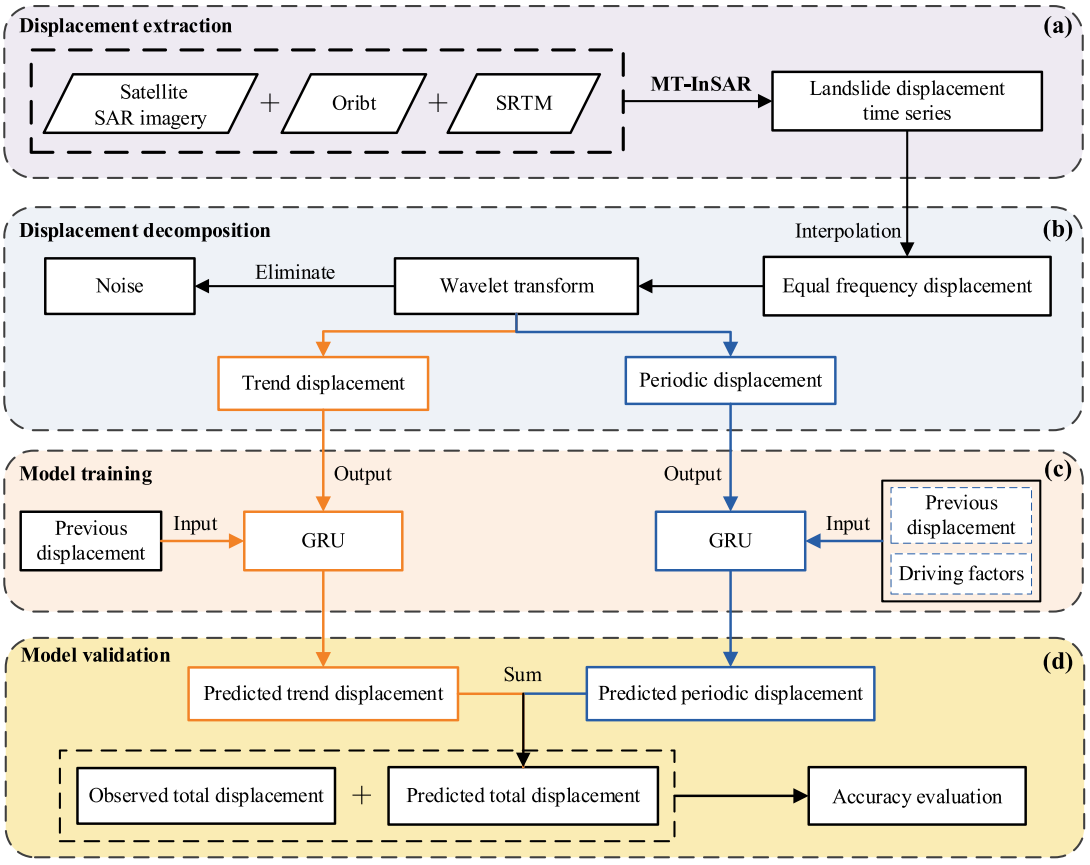

Fig. 4. Framework of the displacement prediction approach: (a) Displacement extraction using MT-InSAR, (b) Displacement decomposition, (c) Model training and (d) Model validation.

3.4.1. *The principle of GRU*

The GRU and LSTM algorithms are both variants of the convolutional neural network (RNN), and GRU is developed on the basis of LSTM neural networks. LSTM is designed to overcome the limitation of RNN by using memory cells. Memory cells have the self-connections that stored the network temporal state (c_t) and controlled through three gates named as: input gate (i_t), output gate (o_t) and forget gate (f_t) (Fig. 5a). The input gate and output gate are used to control the flow of memory cell input (x_t) and outputs (h_t) into the rest of network. The forget gate is added to the memory cell, which passes the output information with high weights from the previous neuron to the next (Shahid et al., 2020). In addition, if the output unit has high activation, then it will pass the information to next neuron. Otherwise, input information with high weights resides in memory cell.

GRU makes the model more simplified and efficient by combining the forget gate and input gate of the LSTM into the update gate, and the memory unit and the hidden layer into the reset gate (Fig. 5b). The reset gate determines which information from the previous steps is to be forgotten which is similar to the function served by the forget gate in LSTM. However, GRU determines the to-be-forgotten information according to the past time steps (in the hidden state (h_{t-1})) which is different from LSTM. The update gate is applied to determine how much of the previous hidden state and how much of the new input should be incorporated into the current hidden state. The performance of GRU is sensitive to its hyperparameters. Adam is a gradient-based optimization algorithm which combines ideas from both gradient descent and momentum (Zhang, 2021; Jiang et al., 2022). Here, Adam is applied to optimize the GRU hyperparameters for accelerating the training process and improve the generalization performance.

3.4.2. *Determination of model inputs*

Precipitation is the primary external triggering of landslide

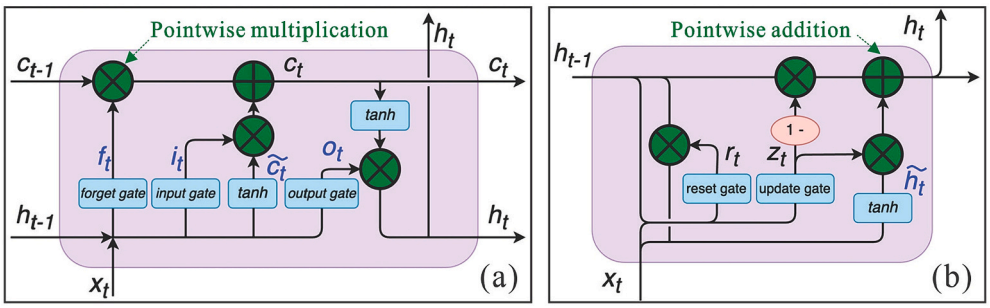

Fig. 5. Conceptual illustrations of (a) LSTM and (b) GRU algorithms, the green circle refers to pointwise operations. (For interpretation of the references to colour in this figure legend, the reader is referred to the web version of this article.)

deformation. Reservoir impoundment of Laxiwa hydropower station destabilized the toppling Guobu slope. Deformation accelerations coincide with the artificial operations. However, after the reservoir water level became leveling-off in 2015, the movements exhibited evident seasonal variations in phase with cyclic rainfall (Shi et al., 2021). In TGRA, Zigui County is in the rainfall center, receiving up to 1,200 mm of the highest rainfall annually. Previous studies argued that landslide deformations in TGRA are mainly influenced by one-month antecedent rainfall (Du et al., 2013; Cao et al., 2016; Zhou et al., 2016). We apply 12-day and 24-day antecedent rainfall as inputs to represent the role of precipitation. Cyclical oscillation of the RWL is another external triggering factor inducing the deformation of reservoir landslides. The seepage force and buoyancy force generated by the fluctuation of the RWL accelerate the deformation of landslide in the TGRA (Tang et al., 2019; Zhou et al., 2022b). With regards to a particular reservoir landslide, the buoyancy force to landslide motion is determined by the RWL elevation, while the seepage force to landslide motion is determined by the fluctuation amplitude of the RWL (Zhou et al., 2018b). We select the average RWL elevation and fluctuation amplitude of every 12-day as model inputs to represent the impact of RWL fluctuation. Landslide deformation is also related to its evolution state. Landslides in different evolution states may show completely different deformation magnitudes even under the same triggering factors. Here we adopt the displacements over the past 12-day, 24-day, and 36-day to represent the current evolution state of landslide.

As stated in Displacement Decomposition (Section 3.3), the trend displacement is mainly controlled by internal geological conditions while the periodic displacement is controlled by external triggers. Hence, three indicators of evolution state are selected as inputs for modeling the trend displacement, and seven indicators of evolution state, rainfall and RWL fluctuation are selected as inputs for modeling the periodic displacement (Table 1).

3.5. Performance evaluation

The accuracy assessment of landslide displacement prediction is important in prediction model establishment. We utilize four accuracy evaluation criteria, namely root mean square error (RMSE), absolute percentage error (APE), and mean absolute percentage error (MAPE) (Table 2). RMSE, APE and MAPE are used to estimate the deviation between the predicted values and the values observed by MT-InSAR. The prediction performance is considered better when the smaller value is obtained among these metrics.

4. Results

We first characterize the spatio-temporal deformation of Shuping and Muyubao landslides applying MT-InSAR extracted time series displacement, and the relationship between deformation and predisposing factors is revealed. Subsequently, we present prediction results for both landslides and evaluate the performance of our proposed ML based prediction method.

Table 1
Inputs of trend and periodic displacement modeling.

Prediction items	Influencing factors	Inputs
Trend displacement	Evolution state	a. the deformation over the past 12 days; b. the deformation over the past 24 days; c. the deformation over the past 36 days.
Periodic displacement	Rainfall	a. the rainfall over the past 12 days; b. the rainfall over the past 24 days.
	RWL fluctuation	c. the variation reservoir level of the past 12 days; d. the average reservoir level of the past 12 days.
	Evolution state	e. the deformation over the past 12 days; f. the deformation over the past 24 days; g. the deformation over the past 36 days.

Table 2
Evaluation criteria for model performance.

Item	Formula	Notes
RMSE	$RMSE = \sqrt{\frac{1}{N}\sum_{i=1}^{N}(\widehat{d}_i - d_i)^2}$	RMSE measures the deviation between the observed and the predicted displacement values, where d_i is the observed values, $\widehat{d}_i$ is the predicted values, and N refers to the number of displacement values.
APE	$APE = \left\|\frac{\widehat{d}_i - d_i}{d_i}\right\|$	Absolute percentage error (APE) is the absolute percentage of the deviation between the observed and the predicted values.
MAPE	$MAPE = \frac{1}{N}\sum_{i=1}^{N}\left\|\frac{d_i - \widehat{d}_i}{d_i}\right\|$	MAPE is the mean of APE. Since the dispersion is absolute value, there will be no cancellation of positive and negative values, MAPE can reflect the error accurately. The smaller value reflected the higher prediction accuracy.

4.1. Deformation characteristics

4.1.1. Shuping landslide

A total of 1018 permanent scattering points were obtained by MT-InSAR. The mean annual velocity of these points is aaproximately −100 mm/year, while the maximum value is −221 mm/year. The landslide deformation velocity shows obvious differences in space. The main deformation zone occurs in the middle and east part of Shuping landslide, while the deformation velocity on the west is not significant (> −80 mm/year) (Fig. 6).

The displacement-time curve of Shuping landslide presents a notable step-like shape (Fig. 6c). In TGRA, the RWL is gradually decreasing from 175 m in March to 159 m by the end of April (Fig. 6b). During this period, the reservoir level declined gradually, while the landslide moved continuously at a small velocity of −7 and − 3 mm/year in 2016 and 2017, respectively (Fig. 7a and g). From May to June every year, the rainy season is coming in TGRA, while the reservoir moves on to the rapid decline period. Under the combined effect of rainfall and reservoir level decline, the landslide is moving rapidly from April to June during the monitoring period, which was shown by the increasing deformation velocity of the MT-InSAR point targets in the sliding area (Fig. 7b and h). The rainfall in TGRA continues to be heavy during July and August, while the reservoir level remains stable at the low level about 145 m. Shuping landslide is moving slowly in this period (Fig. 7c and i), because the stable water level reduces the seepage force on its movement, which is also the major driving factor (Song et al., 2018; Zhou et al., 2022b). The TGRA starts to store water in October, which reaches the storage level of 175 m at the end of October. At the same time, the rainfall decreases gradually. The velocity of the Shuping landslide was relatively small in October compared with the earlier periods (Fig. 7d). Dry season arrives in TGRA from November and lasts until February in the following year when the reservoir level is at the level of 175 m. Under the condition of stable reservoir level and small rainfall from November to February, the landslide moved subtly, which is the most stable period of within the annual monitoring time (Fig. 7e and f).

4.1.2. Muyubao landslide

A total of 1523 points are obtained in Muyubao landslide. The mean velocity of these points is −69 mm/year, and the max velocity is −208 mm/year. Due to the developed cracks in the upper and eastern parts of the landslide, they provide a favorable channel for rainfall infiltration (Zhou et al., 2020). The deformation rate of the landslide decreases gradually from eastern upper portion to the front western portion (Fig. 8). The eastern upper part of the landslide is experiencing significant deformation, with a deformation rate of approximately −100 mm/year. Unlike Shuping landslide, Muyubao landslide keeps moving in the high reservoir level periods (>170 m), such as the 25 mm deformation

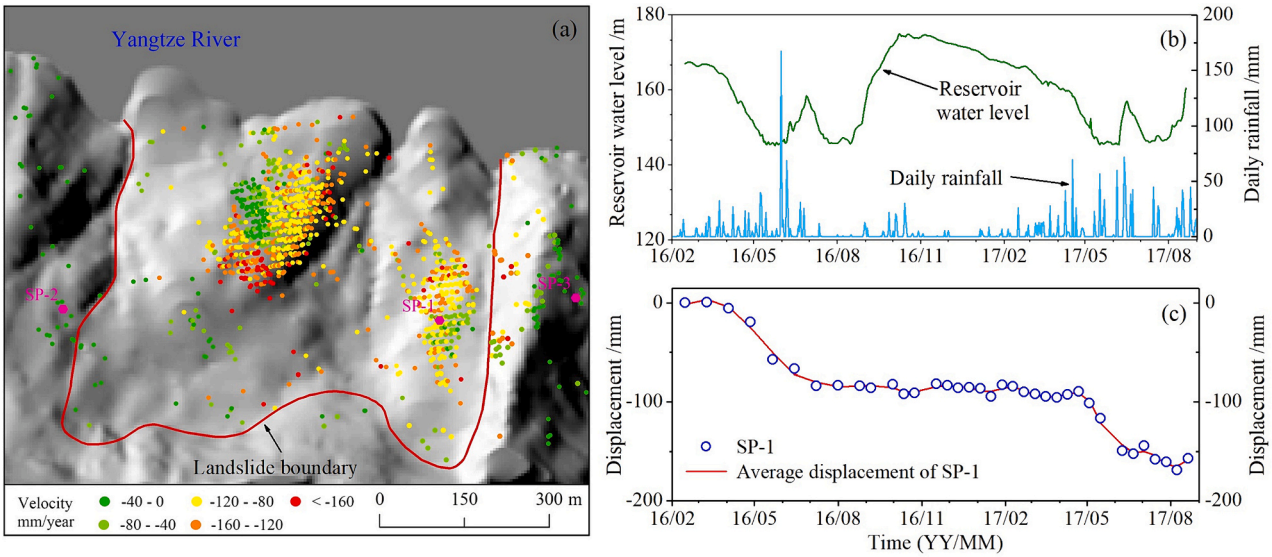

Fig. 6. (a) The deformation velocity of Shuping landslide, (b) Reservoir water level and daily rainfall in TGRA, and (c) The displacement-time curve of SP-1.

from November 2016 and February 2017. The moving speed was slowing down during the slow-decline period (March ~ April 2017), the top monthly speed of which is 10 mm. All the monitoring points on the Muyubao landslide began to accelerate their deformation from May to June 2017. The simultaneously occurred rainy season and rapid drawdown water level of the TGRA triggered a maximum 30 mm/month displacement of the sliding body (Fig. 9). The detailed deformation characteristic description of Muyubao landslide can be found in Zhou et al. (2020).

4.2. Displacement prediction

Here, we select two target points named as SP-1 in Shuping landslide and MYB-1 in Muyubao for displacement prediction, taking into account the high coherence of these points in the SAR images and their strong deformation (Fig. 6 and Fig. 8). The total displacements of both the points are decomposed into trend and period terms by discrete WD algorithm (Fig. 10). In this study, 35 displacement values from March 10, 2016 to April 22, 2017 are used as training samples, while a total of 12 values from May 4, 2017 to September 13, 2017 are used for verification.

4.2.1. Trend displacement

The trend displacements of Shuping and Muyubao landslides are in the pattern of continuous growth. This pattern matches the standard landslide creep curve (Saito, 1965), which indicates that both landslides are in the steady-state creep stage during this monitoring period. Three machine learning methods are used for modeling; the hyperparameters for both landslides are shown in Table 3. The GRU performs well in the prediction of trend displacement (Fig. 11). The RMSE and MAPE of Shuping landslide are 1.332 and 0.007, while they are respectively 2.294, and 0.008 of Muyubao landslide (Table 4).

4.2.2. Periodic displacement

In the periodic displacement modeling, the GRU, LSTM and Kernel-based Extreme Learning Machine (KELM) are selected for modeling. Their hyperparameters are shown in Table 3. The periodic displacement prediction results of the three models for both landslides are shown in Fig. 12, which all have achieved expected results. The RMSE and MAPE of Shuping landslide achieved by GRU are the lowest of 3.716 and 0.321 (Table 4). It suggests GRU achieved the best prediction performance of all the used models. Similarly, GRU also performed best for Muyubao landslide among all considered models. The RMSE and MAPE are 5.414 and 0.354, respectively.

4.2.3. Total displacement

The total displacement is the sum of the predicted trend and periodic values. Accurate prediction of the periodic displacement is the key to the total displacement prediction. In order to compare the model performance in the prediction of the periodic displacement, the trend displacement used to add up to the total displacement is predicted by the same model of GRU. The final prediction results of both landslides are shown in Fig. 13. As shown in Table 4, the total displacement of GRU has the highest accuracy for both landslides, the RMSEs are 3.817 (Shuping landslide) and 5.145 (Muyubao landslide), respectively.

5. Discussion

In this study, we introduced a novel framework for physically-based landslide displacement prediction using MT-InSAR and machine learning techniques. This sectionexamins the physical principles of the movement of Shuping and Muyubao landslides through MT-InSAR analysis. We also analyze the prediction performance of machine learning algorithms and evaluate the monitoring accuracy of MT-InSAR technique quantitatively. Finally, we will discuss the application scenarios of our proposed displacement prediction framework.

5.1. The importance of underlying physical principles behind displacement prediction

Shuping landslide and Muyubao landslide show different deformation modes revealed by using MT-InSAR. As we can see in Fig. 6 and Fig. 8, when the RWL is rapidly declining, the Shuping landslide is experiencing an accelerated motion, which is shown in the rapid rise of displacement monitoring curve. The alternations of accelerated deformations and stabilization phases make the curves a step-like shape. While for Muyubao landslide, in each cycle of reservoir operation, the deformation velocity does not fluctuate much, causing its monitoring curves to follow an approximate linear trend.

According to the shape of the monitoring curves and the reservoir landslide classification criteria proposed by Zhou et al. (2022b), we characterize Shuping landslide and Muyubao landslide as seepage-driven and buoyancy-driven, respectively. The driving mechanisms of RWL fluctuation on the deformation of these two landslides are different due to the variable geological conditions. During the decline period of RWL, as the poor permeability of seepage-driven landslide, the pore-

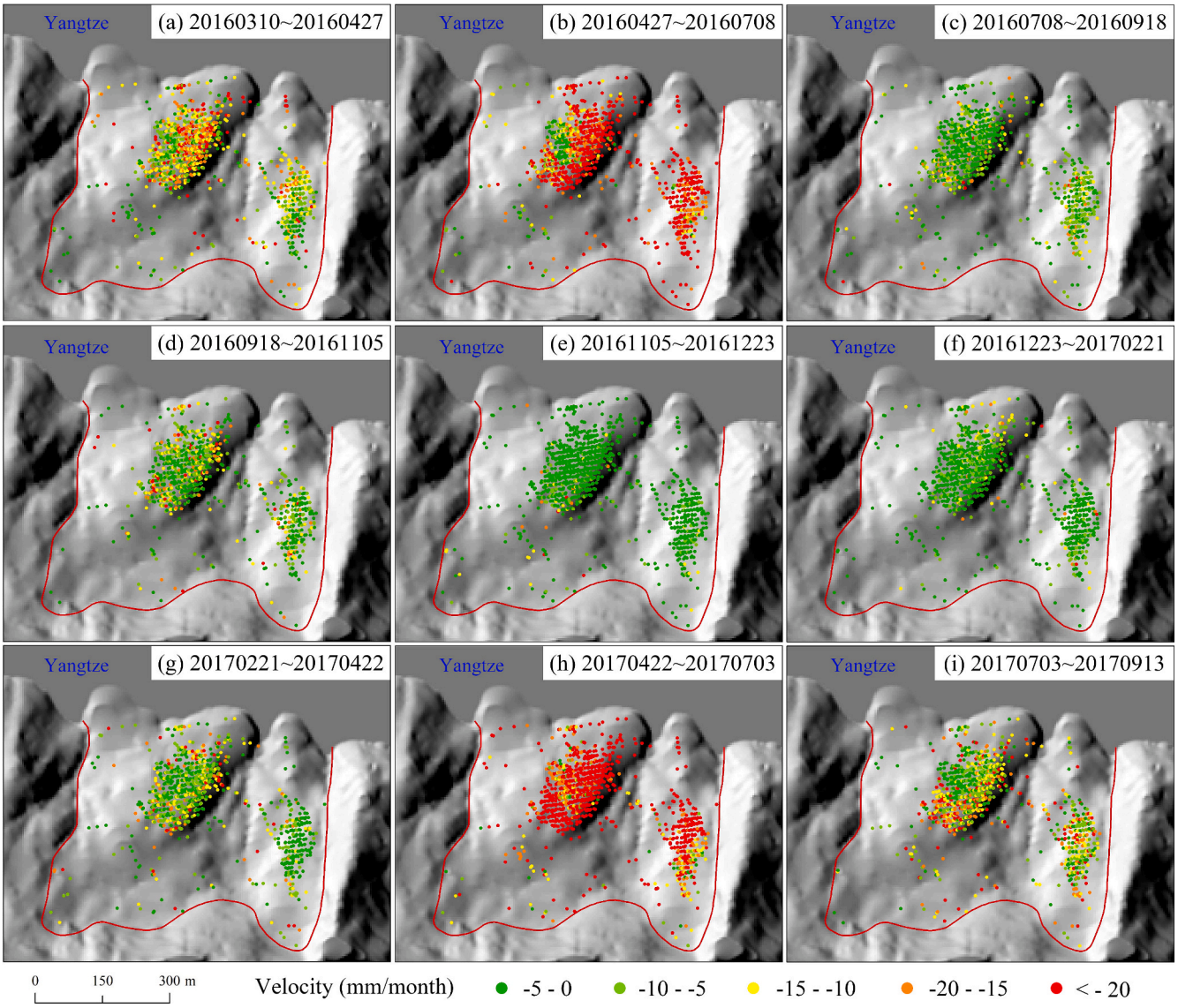

Fig. 7. MT-InSAR-derived monthly deformation velocity map of Shuping landslide.

water pressure dissipates greatly behind the reservoir drawdown speed. The resulting seepage force thus enhances the hydrodynamic pressure within the sliding mass, which makes the strong deformation of the Shuping landslide. The driving force of RWL fluctuation on the Muyubao landslide occurrs during the high RWL period. The buoyancy force reduces the sliding resistance force, thereby triggering the strong deformation of the landslide (Tang et al., 2019). Moreover, rainfall and seepage force act simultaneously on the movement of the Shuping landslide, but they are staggered on the Muyubao landslide. Displacements of both landslides show that their deformations are jointly controlled by rainfall and RWL, which corresponds to the foundations of factors input selection for machine learning modeling. Considering that the effects of external inducing factors on landslide movement are similar on all bank landslides, such as seepage-driven and buoyancy-driven, the inputs used in this study can be generalized to other reservoir landslides in the TGRA and other reservoir regions. But the model needs be retrained based on the specific response mechanisms between factors and deformations.

5.2. Quality of the input displacement

Accurate ground displacement measurement is the precondition for landslide displacement prediction. We verify the accuracy of the displacement data retrieved by MT-InSAR by two methods. In Shuping landslide, two PS points (SP-2 and SP-3, the locations are in Fig. 6a) outside the sliding body are selected for the velocity analysis. According to the displacement time series (Fig. 14a and b), no deformation occurs at either point, the results match the field investigation very well. Moreover, we collect the displacement time series of two GNSS observation points of Shuping landslide in 2017 (the locations are in Fig. 6a), and compare the data obtained by GNSS and MT-InSAR technology. As shown in Fig. 14c and d, the monitored displacements of both techniques are on the same order of magnitude including the sharply changing deformation periods. In Muyubao landslide, the displacement obtained by MT-InSAR is accurate as well (Zhou et al., 2020). The accuracy validation demonstrates that the long-term series of displacement data obtained by open-source radar images and MT-InSAR technology is reliable for landslide prediction.

5.3. Displacement prediction performance using machine learning

The trend terms are relatively easy to predict exactly in both landslides investigated, so the accuracy of the periodic deformation prediction is crucial for their final total displacement prediction. The GRU

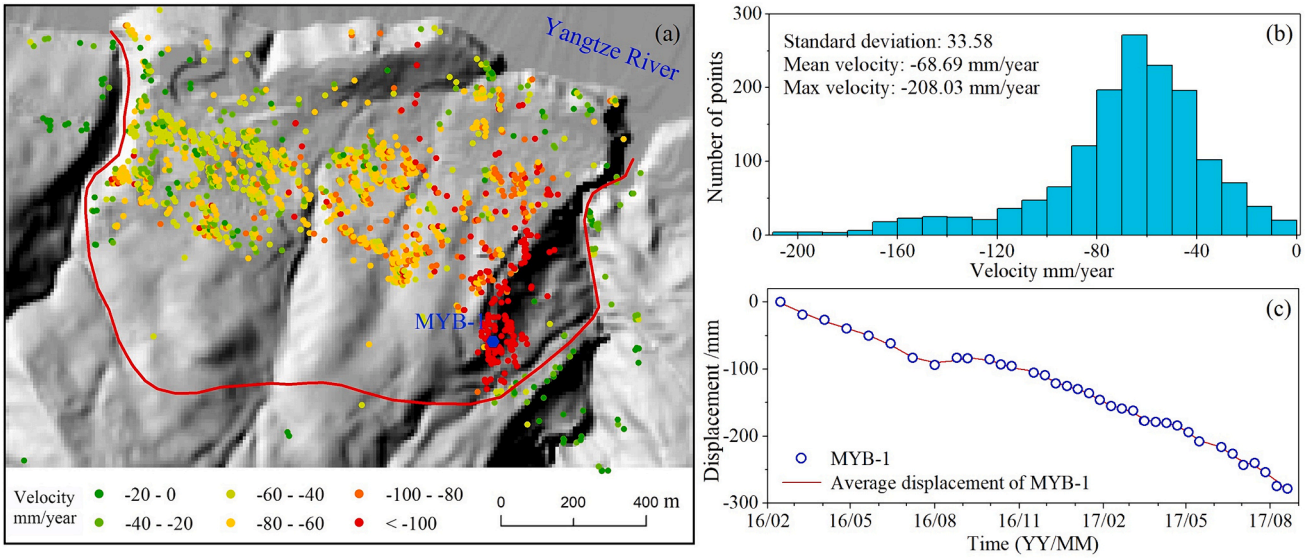

Fig. 8. (a) The deformation velocity of Muyubao landslide, (b) Statistics of deformation velocity, and (c) The displacement-time curve of MYB-1.

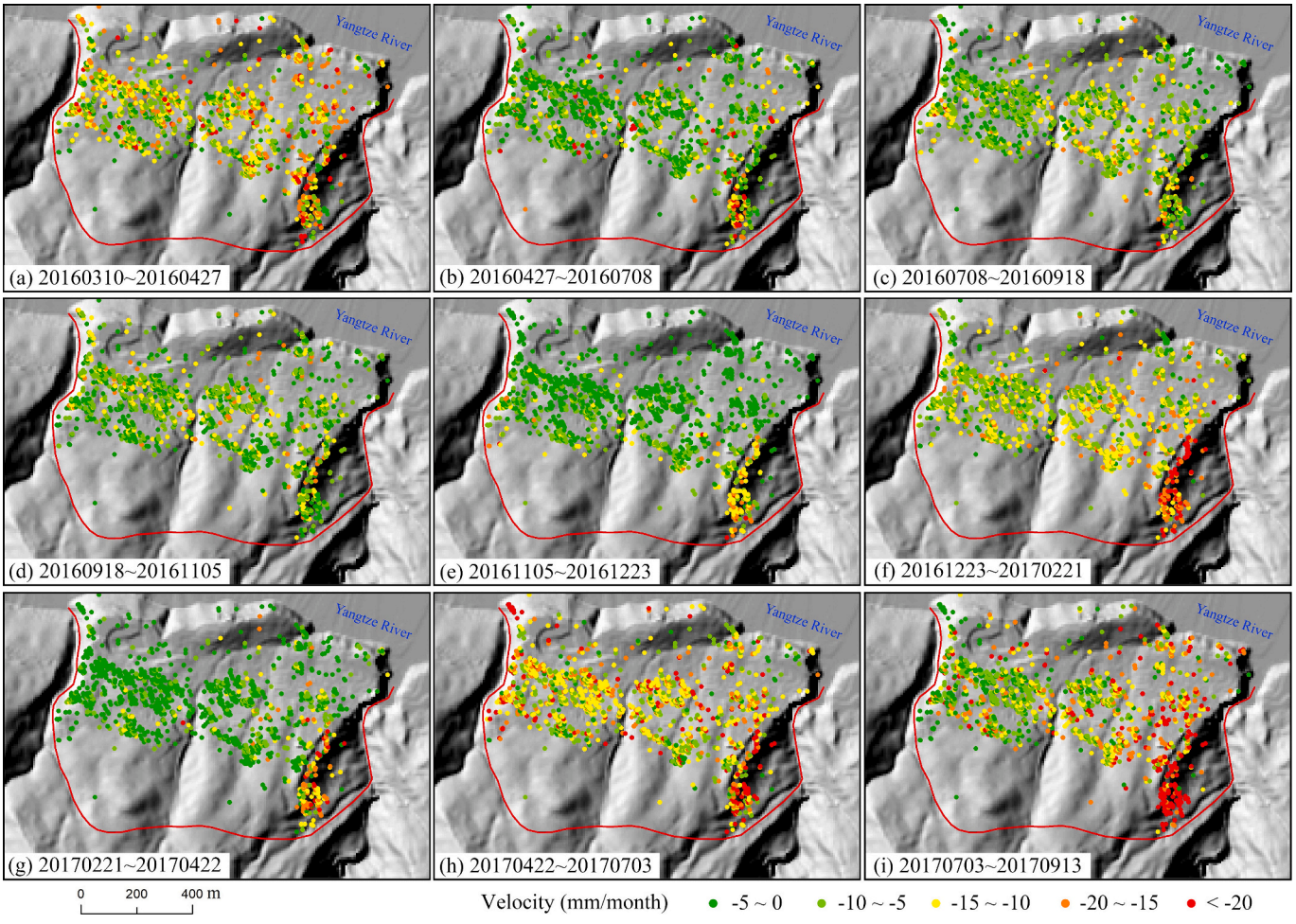

Fig. 9. Monthly deformation velocity of Muyubao landslide from MT-InSAR (After Zhou et al., 2020).

method achieves excellent prediction in this study, and outperforms commonly used LSTM and KELM (Table 4 and Fig. 13). The Adam optimization algorithm can improve the prediction accuracy and speed up the convergence speed in the early stage of the model, while GRU can accurately establish the relationship between the periodic item and their triggers. Due to consideration of physical principles behind landslide deformation, the physically-based method can predict displacement more accurately than pure data-driven methods, especially at the stage

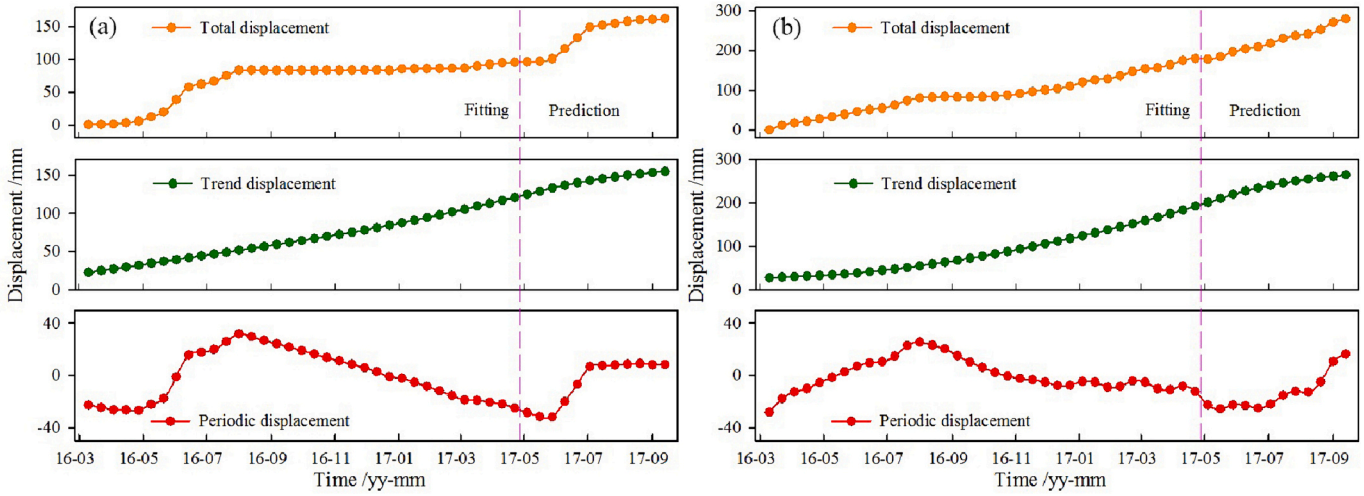

Fig. 10. Displacement decomposition results of (a) Shuping landslide (SP-1), and (b) Muyubao landslide (MYB-1).

Table 3
The main hyperparameters of displacement prediction models.

Modeling	Shuping landslide	Muyubao landslide	Notes
Trend items			Adam is applied as optimizer for GRU and LSTM.
GRU	$n = 4$	$n = 24$	c is the penalty coefficient; γ is the parameter of kernel function;
Periodic items			
GRU	$n = 750$	$n = 520$	n is the number of neurons in hidden layer.
LSTM	$n = 750$	$n = 640$	
KELM	$c = 1010$, $\gamma = 3.65*10^5$	$c = 1010$, $\gamma = 1.38*10^5$	

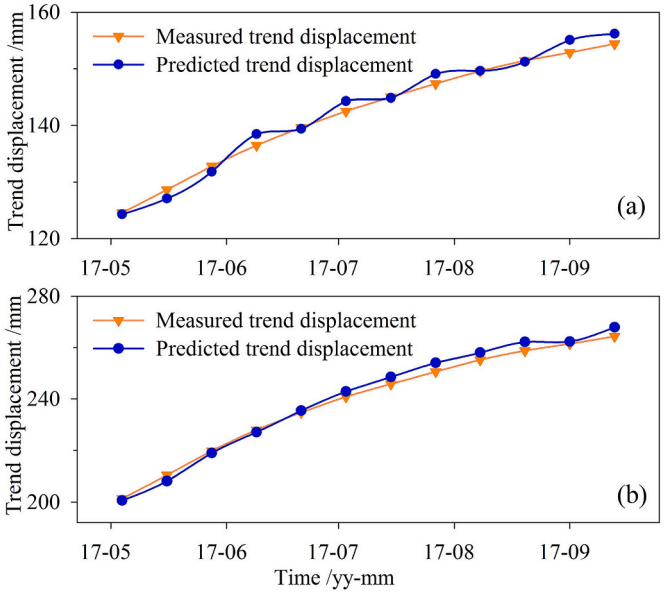

Fig. 11. Prediction results of trend displacement by GRU: (a)Shuping landslide, and (b)Muyubao landslide.

of sudden increase in landslide deformation (Zhou et al., 2018b). For practical applications, the timeliness of the data is also significant for landslide prediction. Due to the hysteresis effect of the displacement influencing factors, the prediction accuracy will be disturbed by long-term historical information over time (that is, the timeliness of the data), which will inevitably lead to the reduction of prediction accuracy. The GRU model proposed in this paper gives full play to the ability of the dynamic model to process relevant information before and after time series mining, which can express the long-term effects of influencing factors. It also performs well in terms of prediction accuracy for cases with limited training samples. ML algorithms obtain knowledge from historical data and construct functions to make forecasts. It assumes that the relationship between the deformation and the triggers does not change. We can achieve an accurate and reliable prediction with ML method only when the future deformation and the historical deformation of a landslide are in the same evolution state. In addition, triggering factors of each landslide and their response relationships to deformation usually change. The inputs and hyperparameters of each landslide prediction model may be different due to the various driving mechanisms. Therefore, we cannot directly apply the prediction model trained in this study to other landslides. It is better to train the model for each target landslide in practice.

5.4. Training strategy and data length in implementation

Applying more data to train machine learning models usually results in a better prediction accuracy. However, for MT-InSAR-driven landslide displacement prediction, we need to balance the effects of MT-InSAR monitoring quality and training data length on prediction accuracy. In previous studies (Du et al., 2013; Xu and Niu, 2018; Ju et al., 2020), the input displacement data were mainly obtained through GNSS, whose performance is almost unaffected by the length of observation period. Since the observation of MT-InSAR is influenced by land-cover type, its observation performance will be affected by the length of observation time to a certain extent. Stable strong scatterers, such as infrastructure, are ideal targets for MT-InSAR observations (Even and Schulz, 2018). In these areas, MT-InSAR can not only extract more monitoring targets, but also make the displacement time series more accurate. Usually, the variation intensity of the land-cover type may be more dramatic over a longer period. Changes in land-cover types result in alterations to the radar echo phase, thereby increasing the likelihood of temporal decorrelation in radar images (Jiang et al., 2014). Additionally, atmospheric effects pose another challenge to retrive reliable measurement points for slow-moving landslides over longer observation periods. Generally, longer observation period would be beneficial for model training, but may result also in more challenges to the monitoring performance of MT-InSAR. The input displacement with high-quality is the prerequisite for an accurate prediction.

To address the influence of training data length on model performance, the displacement from 2017 to 2021 are obtained and applied

Table 4
The statistics of the prediction accuracy.

Model	Index	Shuping landslide			Muyubao landslide		
		Trend displacement	Periodic displacement	Total displacement	Trend displacement	Periodic displacement	Total displacement
GRU	RMSE	1.332	3.716	3.817	2.293	5.414	5.145
	MAPE	0.007	0.321	0.022	0.008	0.354	0.020
LSTM	RMSE	/	4.278	4.423	/	6.023	5.701
	MAPE	/	0.366	0.025	/	0.378	0.023
KELM	RMSE	/	4.101	3.928	/	5.460	5.772
	MAPE	/	0.314	0.026	/	0.374	0.022

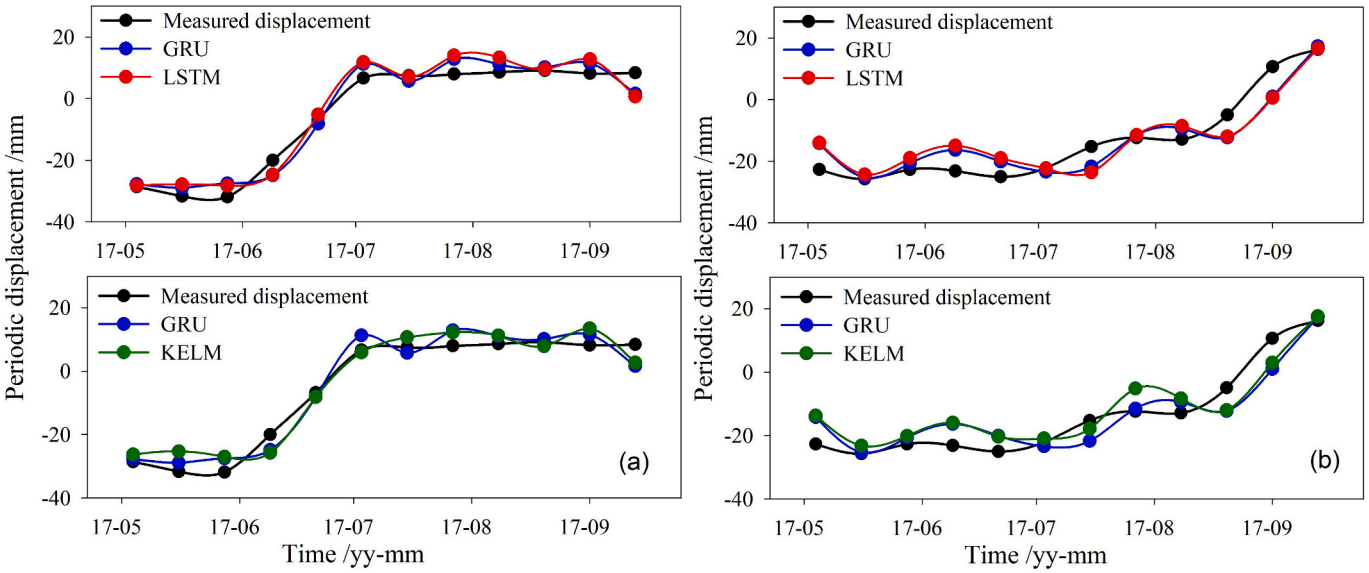

Fig. 12. The periodic displacement prediction: (a) Shuping landslide, and (b) Muyubao landslide.

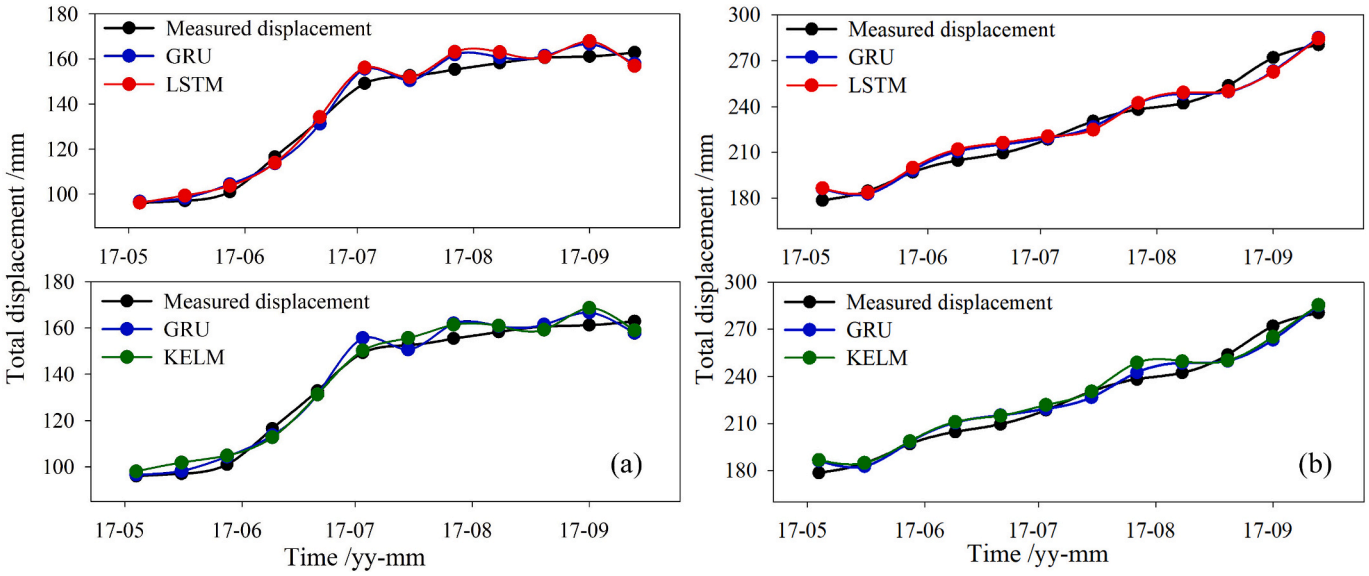

Fig. 13. The total displacement prediction: (a) Shuping landslide, and (b) Muyubao landslide.

for modeling comparison. Here, a neighboring point of MYB-1 is selected for the displacement prediction modeling. A total of 109 displacement data from March 12th, 2017 to October 10th, 2020 are selected for training, while the remaining 31 displacement data from October 22th, 2020 to October 17th, 2021 are used to validation. The RMSE and MAPE of the total displacement prediction are 2.687and 0.853, respectively. Compared with the accuracy results in Table 4, we find that involving more training data does not change the performance much and the improvement in predicton accuracy is not signifcant. Hence, considering the monitoring frequency of Sentinel-1A satellite, the characteristics of MT-InSAR and ML methods, and other related reports (Miao et al., 2018; Zhou et al., 2018b), we suggest that the past data for model training

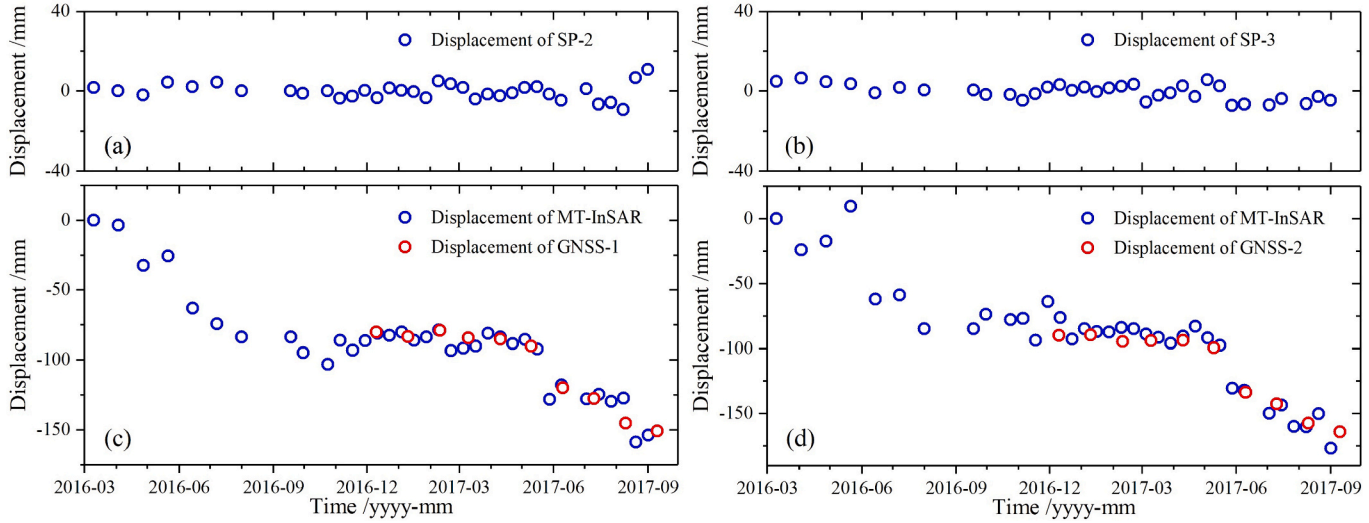

Fig. 14. (a) Displacement time series of SP-2, (b) Displacement time series of SP-3, (c) The comparison of MT-InSAR and GNSS-1, and (d) The comparison of MT-InSAR and GNSS-2. Please see the locations in Fig. 6.

should be more than one year, where 2–5 years is more appropriate.

The performance of a prediction model is time-dependent. A trained model typically exhibits excellent performance on data similarly to what it was trained on. However, the response pattern between deformation and triggering factors changes with the landslide evolution process. The model performance may decrease or even fail when the new response patterns which are not present in its training data occur. In practice, it is necessary to regularly conduct retraining with updated data to ensure the ongoing adaptability to new patterns, thereby maintaining accurate performance of landslide displacement prediction.

5.5. *Application of the MT-InSAR-driven framework*

Since MT-InSAR is effective in monitoring slow deformation, the proposed MT-InSAR-driven approach is more appropriate for the slow-moving progressive landslide prediction. The lifespan of a standard progressive landslide will go through three successive phases: initial deceleration, constant deformation, and accelerate deformation to failure. Secondary creep manifests as slow motion at an almost constant speed over a long period of time, but with fluctuations caused by the inducing factors (rainfall and RWL, et al.). The secondary creep may last for variable duration, which could be months, years, or even decades. The premise to predict the final landslide failure time is to accurately diagnose whether the landslide has moved on to the hyperbolic acceleration state. The ML-based landslide displacement prediction method can be used to identify changes in the deformation state of landslides. The premise to predict the final landslide failure time is to accurately diagnose whether the landslide has moved on to the hyperbolic acceleration state (Intrieri et al., 2019). When a landslide has entered an acceleration state that the ML method cannot predict, it indicates that the landslide enters a next state that is closer to failure. The early warning procedure can be initiated at this time (Zhou et al., 2018b).

SAR satellites' footprints cover most of the globe. Using the open-source Sentinel-1A imagery and the displacement prediction framework developed in this study, we can establish a MT-InSAR-driven regionally oriented monitoring and early warning system for slow-moving landslides. It can provide economic and effective support for global disaster prevention and mitigation, especially for developing countries.

6. Conclusions

In this study, we have developed a robust physically-based framework for predicting landslide displacement prediction by combining MT-InSAR and ML techniques. Our objective is to explore the intricate non-linear relationship between landslide displacement and its trigerring factors. The MT-InSAR method precisely captures the spatio-temporal patterns of displacement fields in both Shuping and Muyubao landslides. Our findings reveal that both landslides are currently in the steady-state creep stage, undergoing deformations characterized by notable spatial variations. Shuping landslide exhibits seepage-driven deformation, primarily triggered by the decline of RWL and short-term concentrated rainfall. On the other hand, Muyubao landslide is buoyancy-driven, with deformation primarily induced by strong rainfall and high water levels. The application of our proposed methodology demonstrates the capability to accurately construct dynamic response patterns between landslide deformation and its triggers. Leveraging three machine learning (ML) models—namely, GRU, LSTM, and KELM—yielded outstanding prediction accuracy. Notably, the Adam algorithm played a pivotal role in optimizing and enhancing the predictive efficiency of the GRU model. Among the models, the GRU model, incorporating influential factors, exhibited the most superior performance. The calculated RMSE and MAPE for the GRU model were 3.817 and 0.022 in Shuping landslide, and 5.145 and 0.020 for the Muyubao landslide, respectively. It is noteworthy that these results were obtained with past data used for model training spanning more than one year, although a training duration of 2–5 years is deemed more appropriate. Furthermore, regularly training with updated data is necessary to maintain accurate performance of prediction model. Overall, our proposed framework for landslide displacement prediction, leveraging freely available Sentinel-1 SAR data, proves to be cost-effective. This approach is particularly recommended for regions susceptible to slow-moving landslides that can be effectively monitored through the MT-InSAR technique.

CRediT authorship contribution statement

Chao Zhou: Writing – original draft, Methodology, Investigation, Funding acquisition, Formal analysis, Data curation, Conceptualization. **Ying Cao:** Writing – original draft, Supervision, Investigation, Funding acquisition, Formal analysis, Conceptualization. **Lulu Gan:** Visualization, Investigation. **Yue Wang:** Visualization. **Mahdi Motagh:** Writing – review & editing, Investigation, Supervision. **Sigrid Roessner:** Writing – review & editing. **Xie Hu:** Writing – review & editing. **Kunlong Yin:** Supervision.

Declaration of competing interest

The authors declare that they have no known competing financial interests or personal relationships that could have appeared to influence the work reported in this paper.

Data availability

Data will be made available on request.

Acknowledgements

This research is funded by the National Natural Science Foundation of China (No. 42371094 No. 41907253, No. 41702330, and No. 42371078) and Key Research and Development Program of Hubei Province (No. 2021BCA219). This work is also partially supported by Helmholtz in Germany within the framework of the HIP project Multi-SaT4SLOWS. We would like to appreciate the editor and two referees for their comments which significantly improves this paper. The first author would like to thank the China Scholarship Council for funding his research at the German Research Centre for Geosciences.

References

Bekaert, D.P.S., Handwerger, A.L., Agram, P., et al., 2020. InSAR-based detection method for mapping and monitoring slow-moving landslides in remote regions with steep and mountainous terrain: an application to Nepal[J]. Remote Sens. Environ. 249, 111983.

Berardino, P., Fornaro, G., Lanari, R., et al., 2002. A new algorithm for surface deformation monitoring based on small baseline differential SAR interferograms[J]. IEEE Trans. Geosci. Remote Sens. 40 (11), 2375–2383.

Cao, Y., Yin, K., Alexander, D.E., et al., 2016. Using an extreme learning machine to predict the displacement of step-like landslides in relation to controlling factors[J]. Landslides 13 (4), 725–736.

Cao, Y., Yin, K., Zhou, C., et al., 2020. Establishment of landslide groundwater level prediction model based on GA-SVM and influencing factor analysis[J]. Sensors 20 (3), 845.

Carla, T., Raspini, F., Intrieri, E., et al., 2016. A simple method to help determine landslide susceptibility from spaceborne InSAR data: the Montescaglioso case study [J]. Environ. Earth Sci. 75 (24), 1–12.

Casagli, N., Intrieri, E., Tofani, V., et al., 2023. Landslide detection, monitoring and prediction with remote-sensing techniques. Nat. Rev. Earth Environ. 4 (1), 51–64.

Chae, B.G., Park, H.J., Catani, F., Simoni, A., Berti, M., 2017 Dec 1. Landslide prediction, monitoring and early warning: a concise review of state-of-the-art[J]. Geosci. J. 21 (6), 1033–1070.

Cheng, W.M., 2014. Research on the Mechanism and Warning Criteria of Landslides Based on Monitoring System after Water Storage in the Three Gorges Reservoir[D]. China University of Geosciences, Wuhan.

Ciampalini, A., Raspini, F., Lagomarsino, D., et al., 2016. Landslide susceptibility map refinement using PSInSAR data[J]. Remote Sens. Environ. 184, 302–315.

Deng, L., Smith, A., Dixon, N., et al., 2021. Machine learning prediction of landslide deformation behaviour using acoustic emission and rainfall measurements[J]. Eng. Geol. 293, 106315.

Devara, M., Tiwari, A., Dwivedi, R., 2021. Landslide susceptibility mapping using MT-InSAR and AHP enabled GIS-based multi-criteria decision analysis[J]. Geomat. Nat. Haz. Risk 12 (1), 675–693.

Du, J., Yin, K., Lacasse, S., 2013. Displacement prediction in colluvial landslides, three Gorges reservoir, China[J]. Landslides 10 (2), 203–218.

Even, M., Schulz, K., 2018. InSAR deformation analysis with distributed scatterers: a review complemented by new advances. Remote Sens. 10 (5), 744.

Fan, X., Yang, F., Siva Subramanian, S., et al., 2020. Prediction of a multi-hazard chain by an integrated numerical simulation approach: the Baige landslide, Jinsha River, China[J]. Landslides 17 (1), 147–164.

Ferretti, A., Prati, C., Rocca, F., 2001. Permanent scatterers in SAR interferometry[J]. IEEE Trans. Geosci. Remote Sens. 39 (1), 8–20.

Ferretti, A., Fumagalli, A., Novali, F., et al., 2011. A new algorithm for processing interferometric data-stacks: SqueeSAR[J]. IEEE Trans. Geosci. Remote Sens. 49 (9), 3460–3470.

Froude, M.J., Petley, D.N., 2018 Aug 23. Global fatal landslide occurrence from 2004 to 2016. Nat. Hazards Earth Syst. Sci. [J]. 18 (8), 2161–2181.

Guo, Z., Chen, L., Gui, L., et al., 2020. Landslide displacement prediction based on variational mode decomposition and WA-GWO-BP model[J]. Landslides 17 (3), 567–583.

Haghshenas Haghighi, M., Motagh, M., 2016. Assessment of ground surface displacement in Taihape landslide, New Zealand, with C-and X-band SAR interferometry[J]. N. Z. J. Geol. Geophys. 59 (1), 136–146.

Han, H., Shi, B., Zhang, L., 2021. Prediction of landslide sharp increase displacement by SVM with considering hysteresis of groundwater change[J]. Eng. Geol. 280, 105876.

Haque, U., Blum, P., Da Silva, P.F., et al., 2016. Fatal landslides in Europe[J]. Landslides 13 (6), 1545–1554.

Helmstetter, A., Sornette, D., Grasso, J.R., et al., 2004. Slider block friction model for landslides: Application to Vaiont and La Clapiere landslides[J]. J. Geophys. Res. Solid Earth 109 (B2).

Hilley, G.E., Burgmann, R., Ferretti, A., et al., 2004. Dynamics of slow-moving landslides from permanent scatterer analysis. Science 304 (5679), 1952–1955.

Hooper, A., 2008. A multi-temporal InSAR method incorporating both persistent scatterer and small baseline approaches[J]. Geophys. Res. Lett. 35 (16).

Hooper, A., Zebker, H.A., 2007. Phase unwrapping in three dimensions with application to InSAR time series[J]. JOSA A 24 (9), 2737–2747.

Hooper, A., Zebker, H., Segall, P., et al., 2004. A new method for measuring deformation on volcanoes and other natural terrains using InSAR persistent scatterers[J]. Geophys. Res. Lett. 31 (23).

Hooper, A., Segall, P., Zebker, H., 2007. Persistent scatterer interferometric synthetic aperture radar for crustal deformation analysis, with application to Volcán Alcedo, Galápagos[J]. J. Geophys. Res. Solid Earth 112 (B7).

Hu, X., Bürgmann, R., Fielding, E.J., et al., 2020. Internal kinematics of the Slumgullion landslide (USA) from high-resolution UAVSAR InSAR data[J]. Remote Sens. Environ. 251, 112057.

Hu, X., Wu, S., Zhang, G., et al., 2021. Landslide displacement prediction using kinematics-based random forests method: a case study in Jinping Reservoir Area, China[J]. Eng. Geol. 283, 105975.

Huang, X., Guo, F., Deng, M., et al., 2020. Understanding the deformation mechanism and threshold reservoir level of the floating weight-reducing landslide in the three Gorges Reservoir Area, China[J]. Landslides 17 (12), 2879–2894.

Intrieri, E., Raspini, F., Fumagalli, A., Lu, P., Del Conte, S., Farina, P., Allievi, J., Ferretti, A., Casagli, N., 2018. The Maoxian landslide as seen from space: detecting precursors of failure with Sentinel-1 data[J]. Landslides 15 (1), 123–133.

Intrieri, E., Carlà, T., Gigli, G., 2019. Forecasting the time of failure of landslides at slope-scale: a literature review[J]. Earth Sci. Rev. 193, 333–349.

Jiang, M., Ding, X., Li, Z., et al., 2014. InSAR coherence estimation for small data sets and its impact on temporal decorrelation extraction. IEEE Trans. Geosci. Remote Sens. 52 (10), 6584–6596.

Jiang, Y., Luo, H., Xu, Q., et al., 2022. A graph convolutional incorporating GRU network for landslide displacement forecasting based on spatiotemporal analysis of GNSS observations [J]. Remote Sens. 14 (4).

Ju, N., Huang, J., He, C., et al., 2020. Landslide early warning, case studies from Southwest China[J]. Eng. Geol. 279, 105917.

Li, H., Xu, Q., He, Y., et al., 2020. Modeling and predicting reservoir landslide displacement with deep belief network and EWMA control charts: a case study in three Gorges Reservoir[J]. Landslides 17 (3), 693–707.

Li, S., Xu, W., Li, Z., 2022. Review of the SBAS InSAR Time-series algorithms, applications, and challenges. Geodesy Geodynam. 13 (2), 114–126.

Lubitz, C., Motagh, M., Wetzel, H.U., et al., 2012. TerraSAR-X Time series uplift monitoring in Staufen, South-West Germany. In: 2012 IEEE International Geoscience and Remote Sensing Symposium. IEEE, pp. 1306–1309.

Mallat, S., 1999. A Wavelet Tour of Signal Processing[M]. Elsevier.

Miao, F., Wu, Y., Xie, Y., et al., 2018. Prediction of landslide displacement with step-like behavior based on multialgorithm optimization and a support vector regression model[J]. Landslides 15 (3), 475–488.

Mohanty, D.K., Parida, A.K., Khuntia, S.S., 2021. Financial market prediction under deep learning framework using auto encoder and kernel extreme learning machine[J]. Appl. Soft Comput. 99, 106898.

Morishita, Y., Lazecky, M., Wright, T.J., et al., 2020. LiCSBAS: an open-source InSAR time series analysis package integrated with the LiCSAR automated Sentinel-1 InSAR processor[J]. Remote Sens. 12 (3), 424.

Motagh, M., Wetzel, H.U., Roessner, S., et al., 2013. A TerraSAR-X InSAR study of landslides in southern Kyrgyzstan, Central Asia[J]. Remote Sens. Lett. 4 (7), 657–666.

Pecoraro, G., Calvello, M., Piciullo, L., 2019. Monitoring strategies for local landslide early warning systems[J]. Landslides 16 (2), 213–231.

Peng, M., Motagh, M., Lu, Z., et al., 2024. Characterization and prediction of InSAR-derived ground motion with ICA-assisted LSTM model. Remote Sens. Environ. 301, 113923.

Rosi, A., Tofani, V., Tanteri, L., et al., 2018. The new landslide inventory of Tuscany (Italy) updated with PS-InSAR: geomorphological features and landslide distribution [J]. Landslides 15 (1), 5–19.

Saito, M., 1965. Forecasting the time of occurrence of a slope failure[C]. In: Proc. 6 th Int. Conf. Soil Mechanics and Foundation Eng., pp. 537–541.

Sassa, K., Tsuchiya, S., Ugai, K., et al., 2009. Landslides: a review of achievements in the first 5 years (2004–2009)[J]. Landslides 6 (4), 275–286.

Shahid, F., Zameer, A., Muneeb, M., 2020. Predictions for COVID-19 with deep learning models of LSTM, GRU and Bi-LSTM. Chaos, Solitons Fractals 140, 110212.

Shi, X., Zhang, L., Zhou, C., et al., 2018. Retrieval of time series three-dimensional landslide surface displacements from multi-angular SAR observations[J]. Landslides 15 (5), 1015–1027.

Shi, X., Hu, X., Sitar, N., et al., 2021. Hydrological control shift from river level to rainfall in the reactivated Guobu slope besides the Laxiwa hydropower station in China[J]. Remote Sens. Environ. 265, 112664.

Song, K., Wang, F., Yi, Q., et al., 2018. Landslide deformation behavior influenced by water level fluctuations of the three Gorges Reservoir (China)[J]. Eng. Geol. 247, 58–68.

Tang, H., Wasowski, J., Juang, C.H., 2019. Geohazards in the three Gorges Reservoir Area, China–Lessons learned from decades of research[J]. Eng. Geol. 261, 105267.

Thiebes, B., Bell, R., Glade, T., et al., 2014. Integration of a limit-equilibrium model into a landslide early warning system[J]. Landslides 11 (5), 859–875.
Wang, W., Motagh, M., Mirzaee, S., et al., 2023. The 21 July 2020 Shaziba landslide in China: results from multi-source satellite remote sensing. Remote Sens. Environ. 295, 113669.
Wasowski, J., Pisano, L., 2020. Long-term InSAR, borehole inclinometer, and rainfall records provide insight into the mechanism and activity patterns of an extremely slow urbanized landslide[J]. Landslides 17 (2), 445–457.
Xia, Z., Motagh, M., Li, T., et al., 2022. The June 2020 Aniangzhai landslide in Sichuan Province, Southwest China: slope instability analysis from radar and optical satellite remote sensing data[J]. Landslides 19 (2), 313–329.
Xu, S., Niu, R., 2018. Displacement prediction of Baijiabao landslide based on empirical mode decomposition and long short-term memory neural network in three Gorges area, China[J]. Comput. Geosci. 111, 87–96.
Xu, Q., Peng, D., Zhang, S., et al., 2020. Successful implementations of a real-time and intelligent early warning system for loess landslides on the Heifangtai terrace, China [J]. Eng. Geol. 278, 105817.
Yang, B., Yin, K., Lacasse, S., et al., 2019. Time series analysis and long short-term memory neural network to predict landslide displacement[J]. Landslides 16 (4), 677–694.
Yin, X., Liu, Q., Huang, X., et al., 2021. Real-time prediction of rockburst intensity using an integrated CNN-Adam-BO algorithm based on microseismic data and its engineering application[J]. Tunn. Undergr. Space Technol. 117, 104133.
Zebker, H.A., Hensley, S., Shanker, P., et al., 2010. Geodetically accurate InSAR data processor. IEEE Trans. Geosci. Remote Sens. 48 (12), 4309–4321.
Zhang, J., 2021. A novel displacement prediction method using gated recurrent unit model with time series analysis in the Erdaohe landslide[J]. Nat. Hazards 105 (1).
Zhang, Y., Meng, X.M., Dijkstra, T.A., et al., 2020. Forecasting the magnitude of potential landslides based on InSAR techniques[J]. Remote Sens. Environ. 241, 111738.
Zhao, C., Kang, Y., Zhang, Q., et al., 2018. Landslide identification and monitoring along the Jinsha River catchment (Wudongde reservoir area), China, using the InSAR method[J]. Remote Sens. 10 (7), 993.
Zheng, H., Duan, M., Sun, X., et al., 2022. Landslide Displacement Prediction based on transfer Learning and Bi-GRU [J]. J. Sens. 12.
Zhou, C., Yin, K., Cao, Y., et al., 2016. Application of time series analysis and PSO–SVM model in predicting the Bazimen landslide in the three Gorges Reservoir, China[J]. Eng. Geol. 204, 108–120.
Zhou, C., Yin, K., Cao, Y., et al., 2018a. A novel method for landslide displacement prediction by integrating advanced computational intelligence algorithms[J]. Sci. Rep. 8 (1), 1–12.
Zhou, C., Yin, K., Cao, Y., et al., 2018b. Displacement prediction of step-like landslide by applying a novel kernel extreme learning machine method[J]. Landslides 15 (11), 2211–2225.
Zhou, C., Cao, Y., Yin, K., et al., 2020. Landslide characterization applying sentinel-1 images and InSAR technique: the Muyubao landslide in the three Gorges Reservoir Area, China[J]. Remote Sens. 12 (20), 3385.
Zhou, C., Cao, Y., Hu, X., Yin, K., Wang, Y., Catani, F., 2022a. Enhanced dynamic landslide hazard mapping using MT-InSAR method in the three Gorges Reservoir Area. Landslides 19 (7), 1585–1597.
Zhou, C., Cao, Y., Yin, K., et al., 2022b. Characteristic comparison of seepage-driven and buoyancy-driven landslides in three Gorges Reservoir area, China[J]. Eng. Geol. 301, 106590.